Article

Thermal Stability and Orthogonal Functionalization of Organophosphonate Self-Assembled Monolayers as Potential Liners for Cu Interconnect

Yu-Wei Chou, Shou-Yi Chang, and Pei Yuin Keng*

Read Online

ACCESS | Metrics & More | Article Recommendations | SI Supporting Information

ABSTRACT: In this study, we investigated the thermal stabilities of butylphosphonic acid (BPA) and aminopropyltriethoxysilane (APTES) self-assembled monolayers (SAM) on a Si substrate. The thermal desorption and the thermal cleavage of the BPA and APTES SAM film on the Si substrate were studied by X-ray photoelectron spectroscopy (XPS) upon thermal treatment from 50 to 550 °C. XPS analyses show that the onset of the thermal desorption of the APTES monolayer occurs at 250 °C and the APTES SAM completely decomposed at 400 °C. Conversely, BPA SAM on Si shows that the onset of thermal desorption occurs at 350 °C, and the BPA SAM completely desorbed at approximately 500 °C. Our study revealed that the organophosphonate SAM is a more stable SAM in modifying the dielectric sidewalls of a Cu interconnect when compared to organosilane SAM. To overcome the spontaneous reaction of the organophosphonate film on the metal substrate, a simple orthogonal functionalization method using thiolate SAM as a sacrificial layer was also demonstrated in this study.

(a) Comparative thermal stability of organosilane and organophosphonate on Si substrate

(b) Orthogonal functionalization
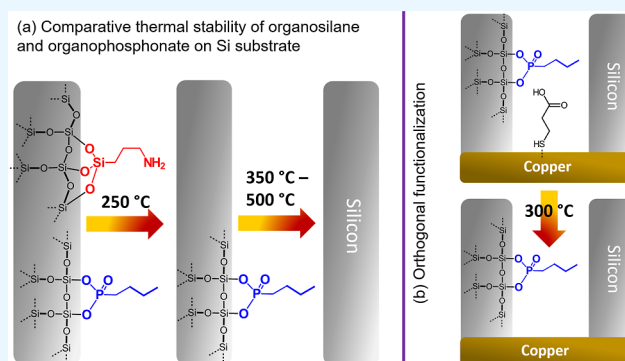
INTRODUCTION

A self-assembled monolayer (SAM) is an effective and versatile functionalization approach for tuning electronic, topography, surface energy, and chemistry at interfaces with a molecular film thickness of 1−3 nm.[1,2] Generally, a SAM molecule can be divided into three parts: (i) the terminal group, which determines the topography and surface energy of the surface, (ii) the aliphatic or aromatic backbones, which provide molecular ordering of the SAM film, and (iii) the anchoring group, which binds to the surface via covalent and noncovalent bonds.[1] Since SAM was first demonstrated in organic field effect transistors,[3] it has been adopted in various applications ranging from biotechnology,[4,5] nanotechnology,[1] and microelectronics.[1,2] Notably, technological advances that drive additive manufacturing, such as microcontact printing,[1,6] constructive lithography,[7,8] and dip-pen lithography,[9] were developed based on the patterning of SAM on micro- and nanostructures. In microelectronics, as the technology node of semiconductor manufacturing approaches a 10 nm length-scale and owing to the increasingly complex three-dimensional (3D) architectures of microelectronic devices,[10] SAM also plays an important role in achieving area selective deposition (ASD),[11−14] acting as a barrier against Cu interdiffusion,[15−17] and acting as a molecular adhesive in Si metallization.[17−19] As a result of the continuous downscaling in the dimensions of trenches and vias, new ultrathin liner materials on Si-based dielectrics that possess both diffusional barrier and adhesive

properties have also garnered significant research interest.[20] As an alternative to conventional inorganic-based liners, ultrathin liners based on the organosilane SAM that are covalently bound on the Si dielectric sidewalls could serve as promising new barrier liners for next-generation back-end-of-line (BEOL) Cu processes.[20] Specifically, organosilane SAM with amino and thiol terminal groups have been investigated as an excellent Cu diffusion barrier owing to its strong interactions of Cu−N and Cu−S chemistry.[15,16,18,21,22] Taking advantage of the strong interaction between the amino-terminated organosilane SAM and a metallic film, this class of SAMs could also serve as a molecular adhesive for strengthening the Cu/Si interface.[17−19] Since the performance of SAM as a passivating layer in ASD, as a Cu diffusion barrier, and as an adhesion layer relies on the formation of two-dimensional (2D) molecularly ordered domains on Si surfaces, a robust and thermally stable SAM is required to withstand the operating temperature of a typical chemical vapor deposition (CVD) or atomic layer deposition (ALD) process.[12,23] Moreover, the deposited SAM needs to withstand numerous cycles of rapid thermal annealing (RTA)

at elevated temperatures in a typical semiconductor processing workflow.[24] These thermal treatments could lead to metal film delamination due to the formation of defects in the liner (organic and inorganic) at the Si dielectric/Cu interface and ultimately result in device failure.[18,25] Thus, the investigation of the thermal stability of SAM on a Si substrate during thermal treatment is of the utmost importance for the utilization of SAM in various applications, including semiconductor packaging processes at elevated temperatures. Although the thermal stability of alkoxysilane SAM has been investigated under ultrahigh vacuum conditions or via in situ X-ray photoelectron spectroscopy (XPS), these environmental conditions are far from a practical semiconductor process.[26–29] One of the earliest studies on the thermal stability of alkoxysilane SAM on Si revealed that alkoxysilane with long hydrocarbon chains detached from the Si surface between 125 and 155 °C of thermal annealing created large holes and aggregates structures based on water contact angle measurement.[30] Other works have shown a much higher thermal stability between 250 and 400 °C, depending on the structure of the organosilane SAM and the thermal annealing condition (in vacuum or in air).[27–29,31] In view of this literature precedence, we present a comprehensive thermal stability study of aminopropyltriethoxysilane (APTES) on Si and evaluate its thermal desorption and bond cleavage with increasing thermal annealing temperature. We also present, for the first time, a comparative thermal stability study of butylphosphonic acid (BPA) as an organophosphonate SAM model compound on Si. Finally, we present a simple orthogonal approach for functionalizing the organophosphonate SAM on Si in the presence of a Cu substrate to mimic the structure of vials at the BEOLs.

In general, the thermal stability of SAMs increases with the increasing number of methylene spacers on the SAM backbone. This is due to the increasing van der Waals interaction between the hydrocarbon chains.[30,32,33] The presence of functional groups—such as the ether, ester, and perfluoroalkyl ether functional groups—along the SAM hydrocarbon backbone is known to induce bond fragmentation at the ether linkage at a lower temperature compared to that of their alkyl counterpart.[34] In addition to the chemical structure and composition of the SAM molecule, the bonding strength between the anchoring group of SAMs and the selected substrate is also critical for determining the thermal stability of the SAM film.[28] For example, a thiolate SAM is thermally more stable compared to a selenoate SAM on the Au(111) surface.[26] An alkoxysilane SAM on Si is also known to be more stable compared to a thiolate SAM on Au.[28] However, a comprehensive comparison of the thermal stability studies of an alkoxysilane SAM and an organophosphonate SAM on Si has never been explored.

Organophosphonate SAMs represent another class of organic monolayers that are widely studied for their functionalization on metal oxides such as Al_2O_3,[11,35–39] TiO_2,[40] HfO_2,[41] and CuO.[42] They have been investigated due to their stronger covalent bonding and high reactivity on metal and metal oxide surfaces.[35] The thermal stability of phosphonic acid SAMs on metal oxide surfaces has been widely investigated under both ambient and reduced pressure conditions. This research has conclusively revealed that the P—O bonding between the phosphonic acid SAM anchoring group and the metal substrate is robust and remains stable up to 800 °C.[27,36,40] The dominant degradation mechanism of this class of SAMs is due to the oxidation or breakage of the alkyl chains on the molecular backbone of SAMs, which has been reported to occur between 200 and 350 °C.[35,36,40] To overcome the lower degradation temperature of an organophosphonate SAM on metal oxides, Wojtecki et al. developed a polymerizable reactive moiety within the organophosphonate SAM to enable covalent bonding between the 2D SAM layer. The lateral cross-linking of organophosphonate SAMs has been shown to be a more effective passivating barrier during AS-ALD of metal oxides on Cu surfaces.[12]

Considering the higher thermal stability of phosphonic acid SAMs on metal oxides, herein we investigate the thermal stability of organophosphonate and alkoxysilane SAMs on Si substrates. To the best of our knowledge, thermal stability of phosphonic acid SAMs on Si has never been explored.[28,29,35] Based on the tethering by the aggregation and growth (T-BAG) method developed by Hanson et al. in the functionalization of organophosphonate film on Si,[43,44] we analyze the thermal cleavage and SAM desorption from the Si substrate via XPS at different thermal annealing temperatures. Moreover, the sample was annealed under a reduced pressure of approximately 20 mTorr, simulating the operating conditions of ALD and RTA that are commonly adapted in semiconductor processing. The thermal annealing conditions applied in this study will be more relevant for industry, as compared to previous reports, when performing thermal stability studies of SAMs in situ in an ultrahigh vacuum environment.[45] Due to the favorable bonding between the phosphonic acid SAM anchoring group with metals and metal oxide substrates, herein, we present an orthogonal deposition approach to achieve selective functionalization of the organophosphonate monolayer film on Si while avoiding the deposition on the adjacent metal substrate. This approach utilizes a thiolate SAM as a sacrificial layer, inhibiting the deposition of a phosphonic acid SAM on the metal substrate. Taking advantage of the well-established chemistry of thiolate SAMs and metal surfaces, along with their thermally labile characteristics, a thiolate SAM was applied to enable an oxide-free Cu-to-Cu bonding in a (dual) damascene process.[46,47] In this approach, a thiolate SAM readily formed a dense 2D-film by creating a strong, thiolate-metal (S—Me) bond, following the dissociation of the S—H bond at room temperature.[46] Subsequently, the organophosphonate SAM layer was selectively functionalized onto the Si substrate. Based on the differences in thermal stability between alkoxysilane- and phosphonic acid-based SAMs, a thiolate SAM was selectively desorbed from the Cu substrate via RTA treatment at 300 °C for 60 min. Under these RTA conditions, the organophosphonate film on Si remained stable, thus enabling nanoengineering at the Si dielectric/metal interface. Our study provides a simple approach for the selective functionalization of a robust organophosphonate film on Si, which simultaneously provides a clean Cu surface for subsequent metal deposition in a Cu (dual) damascene process.

■ EXPERIMENTAL SECTION

Materials and Methods. BPA (Sigma-Aldrich, 99%), APTES (Alfa Aesar, 98%), mercaptopropionic acid (MPA) (Alfa Aesar, 99%), tetrahydrofuran (THF) (Macron, HPLC grade), potassium carbonate (Vetec, 98%), and ethanol (Honeywell, >99.8%) were used as received without further purification. The 3-in. silicon wafer was purchased from Twice Lin Ltd. The copper substrate was deposited by e-gun
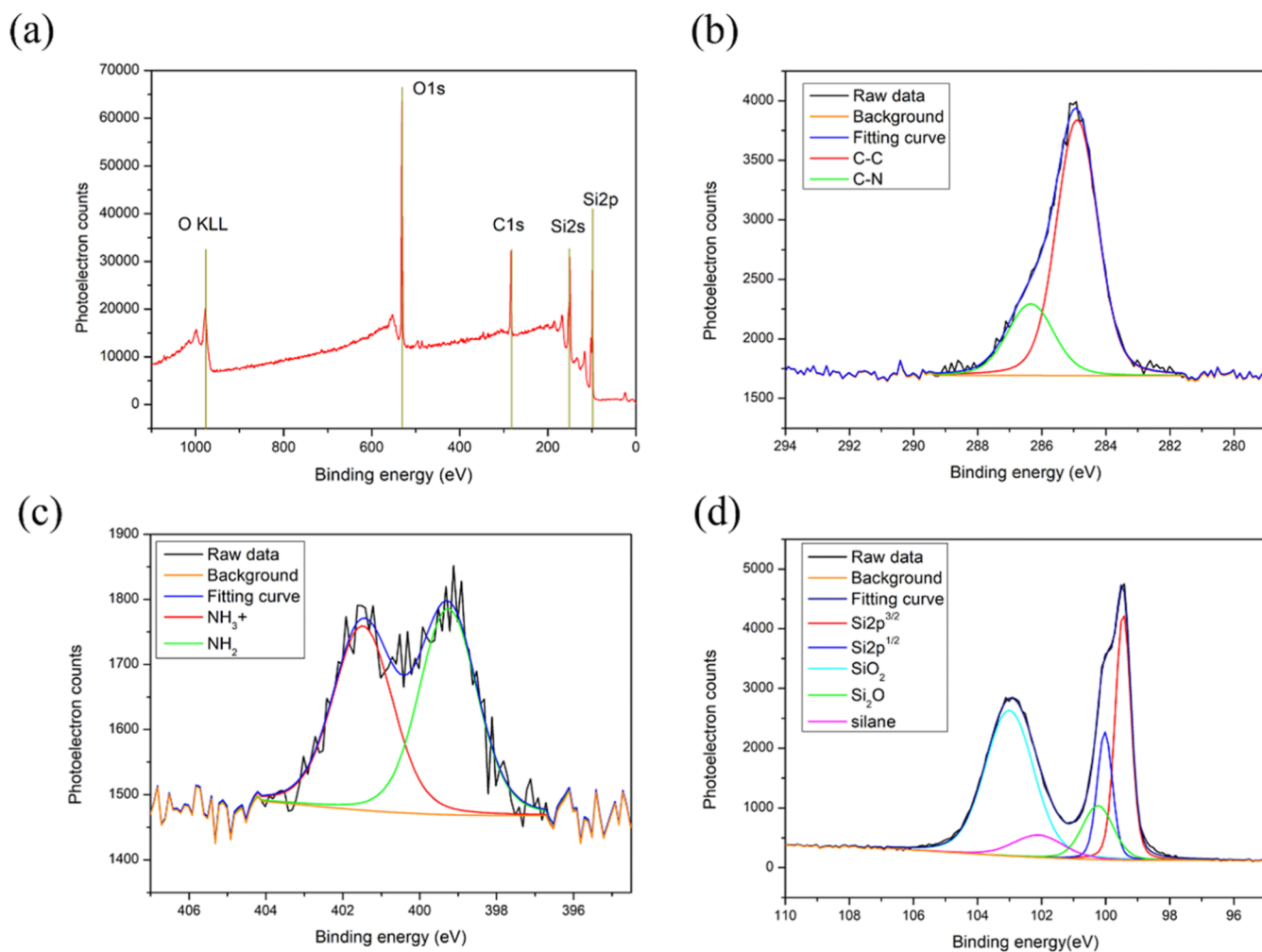
Figure 1. XPS spectra of the (a) full spectrum of a blank silicon and as-deposited APTES SAMs on Si of the (b) C 1s, (c) N 1s, and (d) Si 2p.

(ULVAC) on the Si at the Center for Nanotechnology, Materials Science and Microsystems, NTHU. The molecular sizes of APTES and BPA were simulated using the Merck Molecular Force Field (MMFF94) engine using the Chem Doodle 3D 4.0.1 software. The contribution to the force field includes bond stretching, angle bending, angle stretch-bending, torsions, inversions, van der Waals interactions, and electrostatic interactions.

Substrate Pretreatment and Activation for SAMs of APTES and BPA. A 2 cm × 2 cm coupon of clean single-crystal silicon (100) was prepared by sonicating the wafer in acetone (10 min), isopropyl alcohol (10 min), and then deionized water (10 min). After drying the substrate under a N_2 atmosphere, the activation procedure was subsequently treated by immersing the substrate in piranha solution (3:1 of H_2SO_4/H_2O_2) at 50 °C for 50 min. The substrate was intensively rinsed with deionized water after activation and then finally dried under a N_2 atmosphere and immediately subjected to SAM functionalization.

Deposition of BPA SAM onto the Si Substrate. BPA SAMs were deposited onto an activated Si as described above via the Tethering by Aggregation and Growth (T-BAG) as reported in the literature.[43] Briefly, the activated Si substrate was immersed in a solution of BPA (1 mM) dissolved in THF (30 mL). Then, the solution was placed under ambient conditions to achieve complete evaporation of the solvent and

thus obtain physisorbed BPA on Si. The physisorbed BPA-Si substrate was heated at 140 °C for 2 days in a thermostatic oven under ambient pressure. Upon cooling to room temperature, the BPA-functionalized Si substrate was sonicated in a 2:1 v/v ethanol: water solution of 0.5 M potassium carbonate (13.82 g, 0.1 mol) for 20 min to remove the multilayer BPA film formed on the Si substrate. After the base wash, the sample was dried under N_2 gas. The BPA-functionalized Si substrate was stored under a reduced pressure desiccator.

Deposition of APTES SAM onto the Si Substrate. APTES SAMs were functionalized on activated silicon by immersion in a solution of APTES (0.1 v/v) in toluene for 30 min. After functionalization, the substrate was rinsed with toluene immediately to remove the physisorbed APTES on silicon. The sample was dried under a N_2 atmosphere, and the APTES-functionalized Si substrate was stored in a reduced pressure desiccator. In this study, we assumed the formation of a thin layer of surface native oxides on the Si substrate during handling and experiments in air. For the sake of simplicity, we will refer the Si substrate with native oxides as Si throughout this article.

Thermal Stability of BPA and APTES on the Si Substrate. The thermal stability of the BPA SAM on the Si substrate was tested in a three-zone furnace. Prior to the thermal treatment, the tube furnace was first filled with N_2 gas
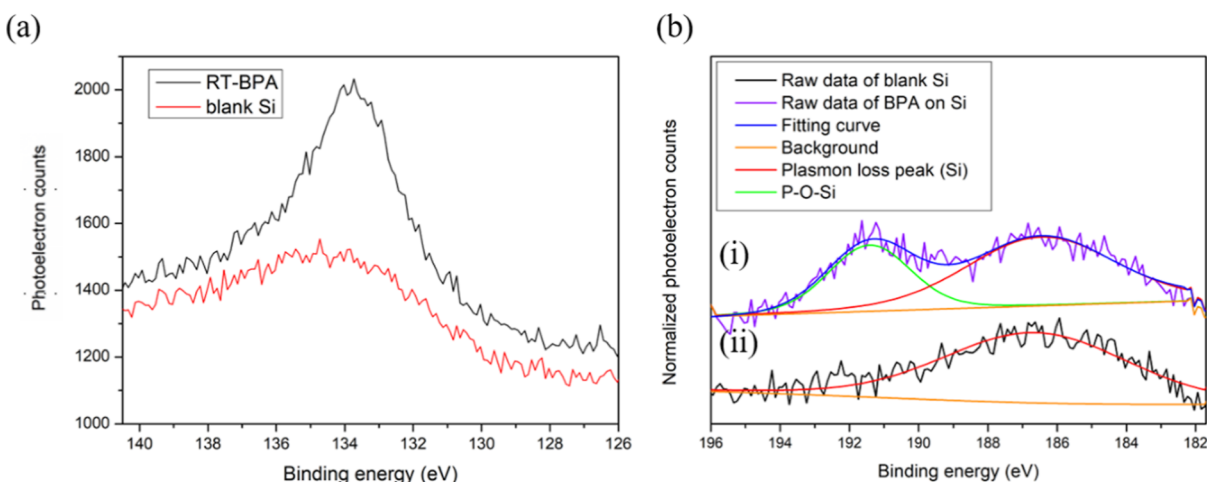
Figure 2. (a) P 2p and (b) P 2s signals in the XPS spectra of (i) BPA SAMs on silicon and (ii) blank silicon substrate at room temperature.

for 10 min. The thermal stability of SAM on Si was investigated by annealing each sample at 50−550 °C for an hour in a tube furnace under a reduced pressure of 6×10^{-3} Torr. The heating rate was set to 5 °C/min. The sample was cooled to room temperature in the nitrogen-filled chamber.

Selective Functionalization of BPA onto Silicon and Copper. Selective functionalization was demonstrated for the copper and silicon substrates. Both substrates were subjected to the same experimental steps to simulate the structure of a via comprised of Si dielectric sidewalls with an underlying metal liner. The Si substrate was pretreated and activated under a similar protocol as described for the functionalization of SAM. The Cu substrate was cleaned with HCL 3.7% for 5 min and then thoroughly rinsed with DI water and finally rinsed with ethanol. Both the cleaned and activated Si and Cu substrates were immersed in 0.005 M MPA. MPA SAM was selectively functionalized on the copper substrate. Upon depositing the MPA sacrificial layer onto the copper substrate, both the MPA SAM-Cu substrate and the Si substrate were subjected to T-BAG deposition conditions to selectively functionalize BPA onto Si (Section 2.3). After SAM functionalization, both the Cu and Si substrates were subjected to RTA at 300 °C for an hour under a reduced pressure of 7 mTorr.

Instrumentation. Prior to characterization, all of the samples were kept in a reduced pressure desiccator and were characterized within 2 weeks to ensure that the SAM film was in a pristine condition. Film thickness analysis was determined using the J.A. Woollam M2000 ellipsometer. For this study, data were collected at 65−75° of incidence and are reported in the 245−1200 nm wavelength interval. The fitting function utilized a transparent film and Cauchy film model to calculate the film thickness. XPS was analyzed via a high-resolution X-ray photoelectron spectrometer (ULVAC-PHI, PHI Quantera II). The photoelectron spectrometer uses the Al Kα source operating at 300 W, and the energy resolution is < 0.48 eV. The base pressure and the operating pressure are $<2.7 \times 10^{-7}$ Torr. An electrical neutralization system uses a dual-source charge compensation system with a low-energy electron beam and a low-energy ion beam with automatic neutralization. For all the XPS data, the binding energy was calibrated to the C 1s peak at 284.8 eV. Curve fitting of XPS line was carried out using CasaXPS software with the Gaussian function with $R^2 >$ 0.99 and U2 Tougaard background subtraction. The thermal

stability test was conducted in a three-zone furnace tube (SJ, T53-906). The thermal annealing temperature was set in the range 50−550 °C for an hour under a reduced pressure of 6×10^{-3} Torr. The RTA process was conducted using the ULVAC-RIKO MILA-5000 under a reduced pressure of 8×10^{-3} Torr.

■ RESULTS AND DISCUSSION

Characterization of APTES-Functionalized Si. In this comparative thermal stability study between organophosphonate SAM and organosilane SAM on Si, we chose to investigate APTES as an organosilane model compound due to their versatility as reactive SAM for postmodification of the base monolayer,[48] as a Cu diffusion barrier,[15−17] as a molecular adhesive at the Cu/Si interface,[17,19] and in enabling area-selective electroless deposition of metal on Si[14,49] in microelectronics applications. XPS analysis of the SAM-functionalized silicon substrate was conducted to confirm the formation of covalent bonding between the SAM and the Si substrate. All XPS spectra were fitted with a Gaussian function with $R^2 >$ 0.99, which is represented by the red and green curves in the XPS spectra for each element. Figure 1a shows the full XPS spectrum of the blank silicon, confirming that the silicon substrate was free of contamination prior to functionalization. Figure 1b,c show the high-resolution XPS spectra of C 1s and N 1s of the as-deposited APTES SAM on the silicon substrate, respectively. The C 1s spectra show an asymmetric peak, which can be deconvoluted into two fitted peaks corresponding to the C−C bonding at 284.8 eV and the C−N bonding at 286.3 eV.[50] The N 1s spectra were fitted with two Gaussian curves corresponding to the uncharged nitrogen at 399.2 eV and the positively charged nitrogen at 401.4 eV.[51] The existence of two different nitrogen species upon deposition of amino-terminated alkoxysilane is consistent with Bierbaum et al.[52] The Si 2p spectra of the APTES-functionalized Si showed two broad peaks centered at binding energies of 99.5 and 103 eV. The former peak can be deconvoluted to three Si species, namely, Si $2p^{1/2}$ (blue curve), Si $2p^{3/2}$ (red curve), and Si_2O (green curve) centered at 100, 99.4,[53−55] and 100.3 eV[55,56] binding energies, respectively. The latter broad peak in Figure 1d can be fitted into two Gaussian curves corresponding to the oxides of the substrates as in SiO_2 bonding at 103 eV[54,57] (cyan−blue curve) and the bonding between the organosilane Si and the inorganic silicon dioxide (Si_{sub}−O−Si_{APTES})
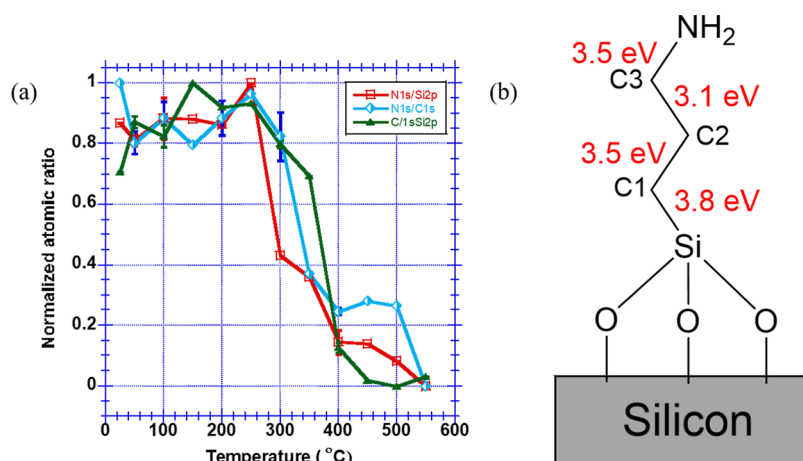
Figure 3. (a) Normalized atomic ratio was determined from the XPS of APTES on silicon as a function of the thermal annealing temperature; (b) schematic drawing of APTES SAM anchored onto a Si substrate.

centered at 102 eV (purple curve).[54,58,59] Based on our systematic optimization, we found that deposition at a low concentration (0.1%) and short immersion time (30 min) is optimal for yielding a 0.6 nm monolayer of APTES SAM based on ellipsometry measurement (Figure S1). Our result is consistent with both a recent report[60] and the simulated molecular size of APTES obtained from the force fields function(Figure S2).

Characterization of BPA-Functionalized Si. For this comparative thermal stability study, BPA was chosen as the organophosphonate model SAM compound due to the similarity in molecular size as the APTES SAM (0.531 nm for BPA and 0.6 nm for APTES) based on force-field simulation. The functionalization of the phosphonic acid SAM on Si has been developed based on a robust technique known as the T-BAG method.[43] Furthermore, the optimization and characterization of the T-BAG process have been thoroughly studied via XPS in the formation of a dense 2D monolayer of organophosphonate on Si.[44] However, a detailed investigation of the thermal stability of organophosphonate SAM on Si has never been explored. The water contact angle measurement for the activated Si substrate before and after BPA functionalization was 43 and 89°, respectively (Figure S3). The increase in the water contact angle can be attributed to the increase in hydrophobicity of the substrate as a result of the methyl terminated moiety of the BPA SAM. Figure 2a shows the P 2p XPS spectra of BPA SAMs modified on Si and a blank Si substrate. Due to the overlapping signal originated from the plasmon loss peak of Si in the P 2p region, it is challenging to confirm the presence of phosphorus through their P 2p spectra. Thus, we performed the high-resolution XPS of the P 2s spectra to confirm the successful deposition of BPA SAMs onto the Si substrate. The P 2s XPS spectra of the (i) BPA modified on Si (purple curve) and (ii) the blank Si substrate (black trace) showed two signals located at 191.4 and 186.4 eV (Figure 2b). The higher binding energy peak can be attributed to the covalent attachment of the phosphonate group onto the Si substrate via P−O−Si bonding that is present only in the BPA modified Si. The other peak at 186.4 eV can be attributed to the plasmon loss peak of silicon, which appeared in both spectra of the BPA modified Si and the blank Si substrate.[44] Therefore, the presence of a signal at 191.4 eV in the P 2s spectra confirmed the formation of BPA SAM on Si via covalent bonding of P−O−Si. The film thickness of the

BPA SAMs was measured to be 0.6 nm via ellipsometry, which is consistent with the theoretical calculation of a single monolayer of BPA (0.531 nm) (Figure S4).

Thermal Stability of APTES and BPA SAMs Functionalized on Si. Alkoxysilane and chlorosilane SAM is the most common class of SAMs used in the functionalization on a Si substrate due to the simple processing condition to obtain covalent bonding between the organic SAM and the inorganic Si substrate.[28] However, the poor thermal stability of silane-based SAM and their tendency to self-polymerize could be detrimental in microelectronic processing.[12,61−63] To overcome the disadvantages of alkoxysilane-based SAM, various groups have investigated phosphonic acid-based SAM for the deposition of a single functional monolayer on Al_2O_3.[35] While the functionalization and thermal stability of phosphonic acid-based SAM have been thoroughly investigated on the Al_2O_3 substrate, the thermal stability of phosphonic acid-SAM on Si has never been explored. Herein, we report the first investigation of the thermal stability of BPA SAM on Si and present a comparative thermal stability study with APTES SAM on Si.

Figure 3 illustrates the thermal desorption spectroscopy studies of APTES SAM. According to the normalized atomic ratio of C/Si and N/Si measured via XPS, the onset of thermal transition of the APTES SAM on Si occurred at 250 °C and complete at 400 °C. At 250 °C, we also observed that the N/Si atomic ratio dropped at a significantly higher rate compared to the reduction of the C/Si atomic ratio from the Si substrate (Figure 3). The difference in the reduction rate of N vs C to Si atomic ratio suggests that the methyl amine fragment first cleaved and desorbed from the Si surface. According to the bond dissociation energy (BDE) determined from density functional theory (DFT) as shown in Figure 3b, we hypothesize that the initial cleavage occurs at the $C_2−C_3$ bond adjacent to the terminal NH_2 group.[64] At 400 °C, the APTES SAM completely decomposed and desorbed from the Si surface. Thus, based on thermal desorption spectroscopy studies of APTES under different thermal annealing temperatures, APTES starts to decompose at 250 °C, which is consistent with previous of literature reports.[15,27,28]

To investigate the thermal stability of BPA on Si, the normalized atomic ratios of P/Si, C/Si, and P/C as a function of the annealing temperature are presented in Figure 4a. Upon thermal annealing of BPA-SAM on Si at 150 °C, the C/Si ratio
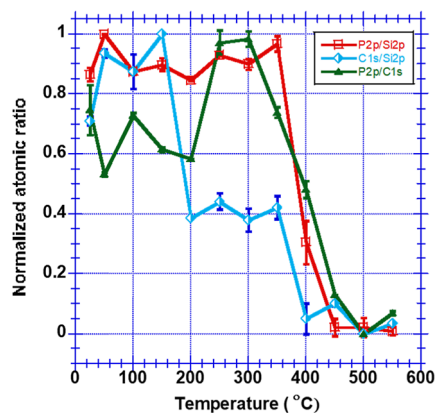
Figure 4. Normalized atomic ratio determined from XPS of BPA on silicon as a function of increasing temperature.

declined drastically, while the P/Si ratio remained constant until 350 °C. This first thermal transition at 150 °C can be attributed to the evaporation of the physiosorbed BPA SAM from the Si surface, while the covalently anchored BPA SAM remained on the Si substrate. The covalently bound BPA SAM remained stable on the SiO_2 surface as the carbon and phosphorus composition remained stable and constant until 350 °C (Figure 4a). Above 350 °C, both the C/Si and P/Si atomic ratios drastically reduced, which indicates that the covalently anchored BPA SAM started to decompose and desorbed from the Si substrate, as shown in Figure 4. Compared to organophosphonate SAM on metal oxide surfaces, the P−O−Metal anchoring group remained stable up to 800 °C.[35] Our study revealed that organophosphonate SAM forms a weaker bonding with the Si substrate but exhibits a higher thermal stability compared with the APTES organosilane SAM in Si.

Summarizing the abovementioned discussion, the phosphonic acid−base SAMs could serve as a candidate for various applications that involve thermal annealing processes, including ASD and Cu/Si interface engineering as a Cu diffusion barrier and as a molecular adhesive that needs to withstand the operating temperature of CVD and ALD. Moreover, short alkyl chain SAM is gaining popularity as a substrate modifier in microelectronics as the dimensional scaling of features at the BEOL continues to shrink. A recent report using dimethyla-minotrimethylsilane has shown promising results as an effective passivating layer on Si toward AS-ALD of several metal films.[65,66] Therefore, our results here provide a rational design for a thermally stable SAM on Si based on an organophosphonate anchoring group. Specifically, organo-phosphonate SAM designed with reactive moieties capable of undergoing photopolymerization,[12] dimerization,[67] and hydro-gen bonding[68] that have elegantly demonstrated enhanced stability and excellent ASD performance can now be adapted on Si-based dielectrics.

Selective Functionalization of BPA on Silicon and Copper Substrates. Organosilane SAM spontaneously self-assembled onto a Si substrate due to the formation of strong covalent Si−O−Si bonding between the organosilane SAM and the underlying substrate.[44,69] Similarly, organophospho-nate is known to spontaneously form strong covalent bonds with various metals upon immersing the metal substrate into the organophosphonate SAM solution.[11,35−38,40−42,70] To overcome the spontaneous functionalization of BPA onto metal oxide surfaces, we demonstrate here an orthogonal functionalization method using MPA as a sacrificial layer.[28] In this approach, the MPA layer first self-assembled into a 2D dense monolayer of protective film on Cu to inhibit the deposition of BPA SAM on Cu.[71] Subsequently, BPA-SAM was functionalized onto the Si substrate via the TBAG method, as described previously. Upon the successful functionalization of BPA on Si, the MPA SAMs on Cu were removed via a simple thermal annealing process at 300 °C, while the BPA-SAM remained intact on the Si substrate. The success of MPA functionalization on Cu was analyzed via XPS of the S 2p spectrum. Figure 5a shows the emergence of an asymmetric peak at 163 eV, which can be deconvoluted into a doublet that correspond to the S−C and Cu−S bonds at 163.8[72] and 162.7 eV,[73,74] respectively. Upon RTA treatment at 300 °C for 60 min, the S−C and Cu−S bonding completely disappeared, as shown in Figure 5b-ii, blue trace).

We have also investigated the need for MPA as a sacrificial layer in inhibiting the deposition of the BPA SAM onto Cu
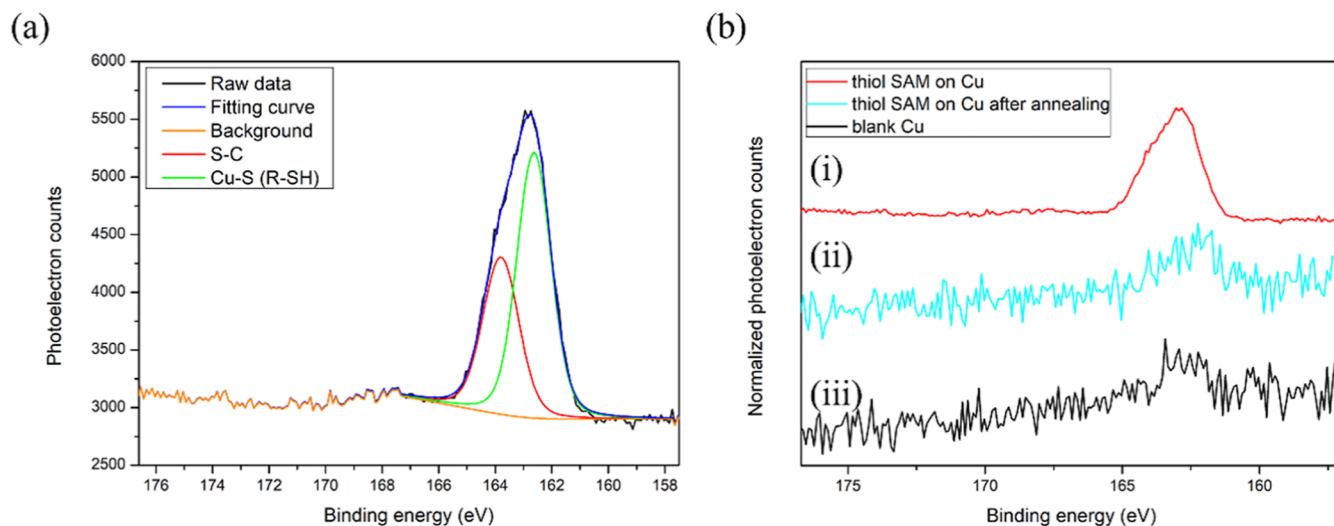

Figure 5. S 2p spectra of (a) MPA SAMs deposited on Cu (b) (i) prior to annealing, (ii) postannealing at 300 °C for 1 h, and (iii) blank Cu without annealing.
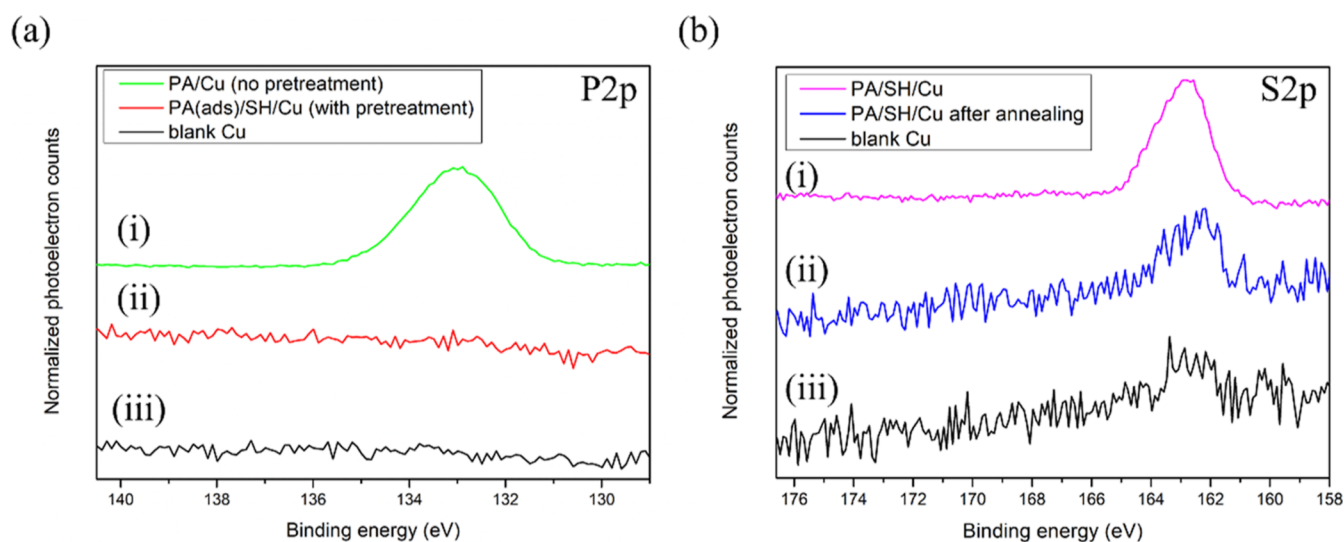
Figure 6. High-resolution XPS spectra of the SAM film on Cu with and without pretreatment with the MPA SAM. (a) Overlaid P 2p spectra (i) BPA SAM on copper with MPA pretreatment (green trace), (ii) BPA on Cu with MPA pretreatment (red trace), and (iii) blank copper (black trace). (b) Overlaid S 2p spectra of (i) MPA SAM-functionalized copper, (ii) removal of the MPA SAM from the Cu substrate via thermal annealing at 300 °C for an hour, and (iii) blank copper.

during a standard T-BAG process. In this study, Cu substrate with and without MPA treatment was immersed in a solution of BPA-SAM in a standard TBAG process. The P 2p XPS spectrum of the Cu substrate without MPA pretreatment as a sacrificial layer showed a symmetric signal at 133.5 eV that corresponded to the P−O/P−O−Cu in Figure 5a (green trace).[75] Meanwhile, no phosphorus-containing compound could be detected via XPS on the Cu substrate that was first pretreated with the MPA sacrificial layer, followed by the T-BAG deposition of BPA as shown in Figure 6a (red trace). The P 2p spectrum resembles the P 2p spectra of a blank Cu substrate, as shown in the stacked P 2p spectra in Figure 6a (black trace). The absence of the P 2p signal can be attributed to the deposition of a protective MPA layer on the Cu substrate, thus inhibiting the functionalization of BPA SAMs on the copper substrate. High-resolution XPS spectra of the S 2p region in the same substrate confirmed the deposition of MPA onto the Cu substrate. The peak at 162.7 eV corresponds to the S−Cu bonding, which confirms the successful deposition of the MPA blocking layer in Figure 6b (purple trace). Finally, the MPA blocking layer was removed from the Cu substrate via RTA treatment in preparation for subsequent metal deposition via either chemical or physical deposition. The successful removal of MPA SAMs is shown in Figure 6b (blue trace), in which the S−Cu bonding in the S 2p spectra disappeared upon RTA treatment, resulting in similar S 2p spectra to a blank Cu substrate (Figure 6b, black trace) Our results here confirm that a simple orthogonal functionalization methodology enabled the selective functionalization of a thermally stable organophosphonate-based SAM on the surface of Si dielectrics, while simultaneously avoiding the deposition on the adjacent Cu substrate.

CONCLUSIONS

The thermal stabilities of BPA and APTES on a Si substrate, as model SAM compounds for organophosphonate and organo-silane monolayer, were investigated in the range 150−550 °C. The substrate was annealed for 60 min under a reduced pressure of 20 mTorr to simulate a more realistic metal

deposition condition. The thermal desorption of the SAM film on Si was monitored by XPS and atomic force microscopy (AFM) after each thermal annealing treatment. This study revealed that the onset decomposition temperature of organosilane SAM on Si was found to be approximately 250 °C, consistent with previous reports. Conversely, the BPA SAM on Si remained stable up to 350 °C Above 350 °C, the P−O−Si anchoring group on the Si substrate began to decompose and completely desorbed from the Si surface at approximately 500 °C.

Our results confirmed that the most commonly used organosilane SAM on Si is not suitable for applications requiring thermal treatment above >250 °C, which is the onset temperature of the thermal desorption of the APTES SAM from Si. Based on our study, organophosphonate SAM could serve as an alternative surface modifier on Si due to their ease of preparation and enhanced film stability compared to conventional organosilane-based SAM. Finally, orthogonal functionalization of the thermally stable organophosphonate SAM onto the surface of dielectrics that simultaneously avoided deposition on the adjacent metal substrate was demonstrated.

■ ASSOCIATED CONTENT

ⓈI Supporting Information

The Supporting Information is available free of charge at https://pubs.acs.org/doi/10.1021/acsomega.3c05629.

> Additional experimental details, including water contact angle, APTES and BPA molecular forced field simulated by MMF94, and AFM image of the blank Si substrate after thermal annealing (PDF)

■ AUTHOR INFORMATION

Corresponding Author

Pei Yuin Keng − *Department of Materials Science and Engineering, National Tsing Hua University, Hsinchu 300, Taiwan;* ⊙ orcid.org/0000-0002-8658-7708; Email: keng.py@gapp.nthu.edu.tw

Authors

Yu-Wei Chou − *Department of Materials Science and Engineering, National Tsing Hua University, Hsinchu 300, Taiwan*

Shou-Yi Chang − *Department of Materials Science and Engineering, National Tsing Hua University, Hsinchu 300, Taiwan;* ⊙ orcid.org/0000-0003-0595-4383

Complete contact information is available at:
https://pubs.acs.org/10.1021/acsomega.3c05629

Author Contributions

The manuscript was written through contributions of all authors. All authors have given approval to the final version of the manuscript.

Notes

The authors declare no competing financial interest.

■ ABBREVIATIONS

2D, two-dimensional; 3D, three-dimensional; AFM, atomic force microscopy; APTES, aminopropyltriethoxysilane; ASD, area selective deposition; Au, gold; BDE, bond dissociation energy; BEOL, back end of line; BPA, butylphosphonic acid; Cu, copper; Cu−N, copper−nitrogen; Cu−S, copper−sulfur; DFT, density functional theory; eV, electronvolt; h, hour; MPA, 3-mercaptopropionic acid; RTA, rapid thermal annealing; SAM, self-assembled monolayer; Si, silicon; S−Me, sulfur−metal; T-BAG, tethering by aggregation and growth; THF, tetrahydrofuran; XPS, X-ray photoelectron spectroscopy

■ REFERENCES

(1) Love, J. C.; Estroff, L. A.; Kriebel, J. K.; Nuzzo, R. G.; Whitesides, G. M. Self-Assembled Monolayers of Thiolates on Metals as a Form of Nanotechnology. *Chem. Rev.* **2005**, *105* (4), 1103−1170.

(2) Casalini, S.; Bortolotti, C. A.; Leonardi, F.; Biscarini, F. Self-Assembled Monolayers in Organic Electronics. *Chem. Soc. Rev.* **2017**, *46* (1), 40−71.

(3) Dimitrakopoulos, C. d.; Malenfant, P. r. l. Organic Thin Film Transistors for Large Area Electronics. *Adv. Mater.* **2002**, *14* (2), 99−117.

(4) Harder, P.; Grunze, M.; Dahint, R.; Whitesides, G. M.; Laibinis, P. E. Molecular Conformation in Oligo(Ethylene Glycol)-Terminated Self-Assembled Monolayers on Gold and Silver Surfaces Determines Their Ability To Resist Protein Adsorption. *J. Phys. Chem. B* **1998**, *102* (2), 426−436.

(5) Gilardi, G.; Fantuzzi, A.; Sadeghi, S. J. Engineering and Design in the Bioelectrochemistry of Metalloproteins. *Curr. Opin. Struct. Biol.* **2001**, *11* (4), 491−499.

(6) Alom Ruiz, S.; Chen, C. S. Microcontact Printing: A Tool to Pattern. *Soft Matter* **2007**, *3* (2), 168−177.

(7) Maoz, R.; Frydman, E.; Cohen, S. R.; Sagiv, J. Constructive Nanolithography": Inert Monolayers as Patternable Templates for In-Situ Nanofabrication of Metal-Semiconductor-Organic Surface Structures—A Generic Approach. *Adv. Mater.* **2000**, *12* (10), 725−731.

(8) Berson, J.; Burshtain, D.; Zeira, A.; Yoffe, A.; Maoz, R.; Sagiv, J. Single-Layer Ionic Conduction on Carboxyl-Terminated Silane Monolayers Patterned by Constructive Lithography. *Nat. Mater.* **2015**, *14* (6), 613−621.

(9) Piner, R. D.; Zhu, J.; Xu, F.; Hong, S.; Mirkin, C. A. Dip-Pen" Nanolithography. *Science* **1999**, *283* (5402), 661−663.

(10) Biswas, A.; Bayer, I. S.; Biris, A. S.; Wang, T.; Dervishi, E.; Faupel, F. Advances in Top-down and Bottom-up Surface Nanofabrication: Techniques, Applications & Future Prospects. *Adv. Colloid Interface Sci.* **2012**, *170* (1−2), 2−27.

(11) Bobb-Semple, D.; Nardi, K. L.; Draeger, N.; Hausmann, D. M.; Bent, S. F. Area-Selective Atomic Layer Deposition Assisted by Self-Assembled Monolayers: A Comparison of Cu, Co, W, and Ru. *Chem. Mater.* **2019**, *31* (5), 1635−1645.

(12) Wojtecki, R.; Mettry, M.; Fine Nathel, N. F.; Friz, A.; De Silva, A.; Arellano, N.; Shobha, H. Fifteen Nanometer Resolved Patterns in Selective Area Atomic Layer Deposition—Defectivity Reduction by Monolayer Design. *ACS Appl. Mater. Interfaces* **2018**, *10* (44), 38630−38637.

(13) Zyulkov, I.; Krishtab, M.; De Gendt, S.; Armini, S. Selective Ru ALD as a Catalyst for Sub-Seven-Nanometer Bottom-Up Metal Interconnects. *ACS Appl. Mater. Interfaces* **2017**, *9* (36), 31031−31041.

(14) Zyulkov, I.; Armini, S.; Opsomer, K.; Detavernier, C.; De Gendt, S. Selective Electroless Deposition of Cobalt Using Amino-Terminated SAMs. *J. Mater. Chem. C* **2019**, *7* (15), 4392−4402.

(15) Caro, A. M.; Armini, S.; Richard, O.; Maes, G.; Borghs, G.; Whelan, C. M.; Travaly, Y. Bottom-Up Engineering of Subnanometer Copper Diffusion Barriers Using NH2-Derived Self-Assembled Monolayers. *Adv. Funct. Mater.* **2010**, *20* (7), 1125−1131.

(16) Zhang, Y.-P.; Chandra Sil, M.; Chen, C.-M. Organosiloxane Nanolayer as Diffusion Barrier for Cu Metallization on Si. *Appl. Surf. Sci.* **2021**, *567*, 150800.

(17) Chung, Y.; Lee, S.; Mahata, C.; Seo, J.; Lim, S.-M.; Jeong, M.; Jung, H.; Joo, Y.-C.; Park, Y.-B.; Kim, H.; Lee, T. Coupled Self-Assembled Monolayer for Enhancement of Cu Diffusion Barrier and Adhesion Properties. *RSC Adv.* **2014**, *4* (104), 60123−60130.

(18) Wu, P.-H.; Lai, Y.-Z.; Zhang, Y.-P.; Sil, M. C.; Lee, P.-H. H.; Wei, T.-C.; Chen, C.-M. Organosiloxane Monolayers Terminated with Amine Groups as Adhesives for Si Metallization. *ACS Appl. Nano Mater.* **2020**, *3* (4), 3741−3749.

(19) Bogan, J.; Brady-Boyd, A.; Armini, S.; Lundy, R.; Selvaraju, V.; O'Connor, R. Nucleation and Adhesion of Ultra-Thin Copper Films on Amino-Terminated Self-Assembled Monolayers. *Appl. Surf. Sci.* **2018**, *462*, 38−47.

(20) Mikami, N.; Hata, N.; Kikkawa, T.; Machida, H. Robust Self-Assembled Monolayer as Diffusion Barrier for Copper Metallization. *Appl. Phys. Lett.* **2003**, *83* (25), 5181−5183.

(21) Ganesan, P. G.; Kumar, A.; Ramanath, G. Surface Oxide Reduction and Bilayer Molecular Assembly of a Thiol-Terminated Organosilane on Cu. *Appl. Phys. Lett.* **2005**, *87* (1), 011905.

(22) Krishnamoorthy, A.; Chanda, K.; Murarka, S. P.; Ramanath, G.; Ryan, J. G. Self-Assembled near-Zero-Thickness Molecular Layers as Diffusion Barriers for Cu Metallization. *Appl. Phys. Lett.* **2001**, *78* (17), 2467−2469.

(23) Leskelä, M.; Ritala, M. Atomic Layer Deposition Chemistry: Recent Developments and Future Challenges. *Angew. Chem., Int. Ed.* **2003**, *42* (45), 5548−5554.

(24) Lord, H. A. Thermal and Stress Analysis of Semiconductor Wafers in a Rapid Thermal Processing Oven. *IEEE Trans. Semicond. Manuf.* **1988**, *1* (3), 105−114.

(25) Song, S.; Liu, Y.; Li, M.; Mao, D.; Chang, C.; Ling, H. Diffusion Barrier Performance of W/Ta-W-N Double Layers for Cu Metallization. *Microelectron. Eng.* **2006**, *83* (3), 423−427.

(26) Ossowski, J.; Nascimbeni, G.; Żaba, T.; Verwüster, E.; Rysz, J.; Terfort, A.; Zharnikov, M.; Zojer, E.; Cyganik, P. Relative Thermal Stability of Thiolate- and Selenolate-Bonded Aromatic Monolayers on the Au(111) Substrate. *J. Phys. Chem. C* **2017**, *121* (50), 28031−28042.

(27) Bhairamadgi, N. S.; Pujari, S. P.; Trovela, F. G.; Debrassi, A.; Khamis, A. a. M.; Alonso, J. M.; Al Zahrani, A. A.; Wennekes, T.; Al-Turaif, H. A.; van Rijn, C.; Alhamed, Y. A.; Zuilhof, H. Hydrolytic and Thermal Stability of Organic Monolayers on Various Inorganic Substrates. *Langmuir* **2014**, *30* (20), 5829−5839.

(28) Chandekar, A.; Sengupta, S. K.; Whitten, J. E. Thermal Stability of Thiol and Silane Monolayers: A Comparative Study. *Appl. Surf. Sci.* **2010**, *256* (9), 2742−2749.

(29) Kulkarni, S. A.; Mirji, S. A.; Mandale, A. B.; Vijayamohanan, K. P. Thermal Stability of Self-Assembled Octadecyltrichlorosilane Monolayers on Planar and Curved Silica Surfaces. *Thin Solid Films* **2006**, *496* (2), 420−425.

(30) Calistri-Yeh, M.; Kramer, E. J.; Sharma, R.; Zhao, W.; Rafailovich, M. H.; Sokolov, J.; Brock, J. D. Thermal Stability of Self-Assembled Monolayers from Alkylchlorosilanes. *Langmuir* **1996**, *12* (11), 2747−2755.

(31) Srinivasan, U.; Houston, M. R.; Howe, R. T.; Maboudian, R. Alkyltrichlorosilane-Based Self-Assembled Monolayer Films for Stiction Reduction in Silicon Micromachines. *J. Microelectromech. Syst.* **1998**, *7* (2), 252−260.

(32) Fukushima, H.; Seki, S.; Nishikawa, T.; Takiguchi, H.; Tamada, K.; Abe, K.; Colorado, R.; Graupe, M.; Shmakova, O. E.; Lee, T. R. Microstructure, Wettability, and Thermal Stability of Semifluorinated Self-Assembled Monolayers (SAMs) on Gold. *J. Phys. Chem. B* **2000**, *104* (31), 7417−7423.

(33) Kim, T.; Chan, K. C.; Crooks, R. M. Polymeric Self-Assembled Monolayers. 4. Chemical, Electrochemical, and Thermal Stability of ω-Functionalized, Self-Assembled Diacetylenic and Polydiacetylenic Monolayers. *J. Am. Chem. Soc.* **1997**, *119* (1), 189−193.

(34) Schönherr, H.; Ringsdorf, H.; Jaschke, M.; Butt, H.-J.; Bamberg, E.; Allinson, H.; Evans, S. D. Self-Assembled Monolayers of Symmetrical and Mixed Alkyl Fluoroalkyl Disulfides on Gold. 2. Investigation of Thermal Stability and Phase Separation. *Langmuir* **1996**, *12* (16), 3898−3904.

(35) Wan, X.; Lieberman, I.; Asyuda, A.; Resch, S.; Seim, H.; Kirsch, P.; Zharnikov, M. Thermal Stability of Phosphonic Acid Self-Assembled Monolayers on Alumina Substrates. *J. Phys. Chem. C* **2020**, *124* (4), 2531−2542.

(36) Chen, D.; Yin Wu, H. K.; Naderi-Gohar, S.; Wu, Y.; Huang, Y.; Nie, H.-Y. An Extremely Rapid Dip-Coating Method for Self-Assembly of Octadecylphosphonic Acid and Its Thermal Stability on an Aluminum Film. *J. Mater. Chem. C* **2014**, *2* (46), 9941−9948.

(37) Seo, S.; Yeo, B. C.; Han, S. S.; Yoon, C. M.; Yang, J. Y.; Yoon, J.; Yoo, C.; Kim, H.; Lee, Y.; Lee, S. J.; Myoung, J.-M.; Lee, H.-B.-R.; Kim, W.-H.; Oh, I.-K.; Kim, H. Reaction Mechanism of Area-Selective Atomic Layer Deposition for Al2O3 Nanopatterns. *ACS Appl. Mater. Interfaces* **2017**, *9* (47), 41607−41617.

(38) Gothe, B.; de Roo, T.; Will, J.; Unruh, T.; Mecking, S.; Halik, M. Self-Assembled Monolayer Field-Effect Transistors Based on Oligo-9,9′-Dioctylfluorene Phosphonic Acids. *Nanoscale* **2017**, *9* (47), 18584−18589.

(39) Hatt, T.; Bartsch, J.; Davis, V.; Richter, A.; Kluska, S.; Glunz, S. W.; Glatthaar, M.; Fischer, A. Hydrophobic AlOₓ Surfaces by Adsorption of a SAM on Large Areas for Application in Solar Cell Metallization Patterning. *ACS Appl. Mater. Interfaces* **2021**, *13* (4), 5803−5813.

(40) Kanta, A.; Sedev, R.; Ralston, J. The Formation and Stability of Self-Assembled Monolayers of Octadecylphosphonic Acid on Titania. *Colloids Surf., A* **2006**, *291* (1−3), 51−58.

(41) Acton, B. O.; Ting, G. G.; Shamberger, P. J.; Ohuchi, F. S.; Ma, H.; Jen, A. K.-Y. Dielectric Surface-Controlled Low-Voltage Organic Transistors via n-Alkyl Phosphonic Acid Self-Assembled Monolayers on High-k Metal Oxide. *ACS Appl. Mater. Interfaces* **2010**, *2* (2), 511−520.

(42) Hoque, E.; DeRose, J. A.; Bhushan, B.; Hipps, K. W. Low Adhesion, Non-Wetting Phosphonate Self-Assembled Monolayer Films Formed on Copper Oxide Surfaces. *Ultramicroscopy* **2009**, *109* (8), 1015−1022.

(43) Hanson, E. L.; Schwartz, J.; Nickel, B.; Koch, N.; Danisman, M. F. Bonding Self-Assembled, Compact Organophosphonate Monolayers to the Native Oxide Surface of Silicon. *J. Am. Chem. Soc.* **2003**, *125* (51), 16074−16080.

(44) Gouzman, I.; Dubey, M.; Carolus, M. D.; Schwartz, J.; Bernasek, S. L. Monolayer vs. Multilayer Self-Assembled Alkylphosphonate Films: X-Ray Photoelectron Spectroscopy Studies. *Surf. Sci.* **2006**, *600* (4), 773−781.

(45) Barreca, D.; Carraro, G.; Warwick, M. E. A.; Kaunisto, K.; Gasparotto, A.; Gombac, V.; Sada, C.; Turner, S.; Van Tendeloo, G.; Maccato, C.; Fornasiero, P. Fe 2 O 3 -TiO 2 Nanosystems by a Hybrid PE-CVD/ALD Approach: Controllable Synthesis, Growth Mechanism, and Photocatalytic Properties. *CrystEngComm* **2015**, *17* (32), 6219−6226.

(46) Vericat, C.; Vela, M. E.; Corthey, G.; Pensa, E.; Cortés, E.; Fonticelli, M. H.; Ibañez, F.; Benitez, G. E.; Carro, P.; Salvarezza, R. C. Self-Assembled Monolayers of Thiolates on Metals: A Review Article on Sulfur-Metal Chemistry and Surface Structures. *RSC Adv.* **2014**, *4* (53), 27730−27754.

(47) Maestre Caro, A.; Travaly, Y.; Beyer, G.; Tokei, Z.; Maes, G.; Borghs, G.; Armini, S. Selective Self-Assembled Monolayer Coating to Enable Cu-to-Cu Connection in Dual Damascene Vias. *Microelectron. Eng.* **2013**, *106*, 76−80.

(48) Haensch, C.; Hoeppener, S.; Schubert, U. S. Chemical Modification of Self-Assembled Silane Based Monolayers by Surface Reactions. *Chem. Soc. Rev.* **2010**, *39* (6), 2323−2334.

(49) Glickman, E.; Inberg, A.; Fishelson, N.; Shaham-Diamand, Y. Electroless Deposition and Electrical Resistivity of Sub-100nm Cu Films on SAMs: State of the Art. *Microelectron. Eng.* **2007**, *84* (11), 2466−2470.

(50) Yan, X.; Xu, T.; Chen, G.; Yang, S.; Liu, H.; Xue, Q. Preparation and Characterization of Electrochemically Deposited Carbon Nitride Films on Silicon Substrate. *J. Phys. D: Appl. Phys.* **2004**, *37* (6), 907−913.

(51) Ederer, J.; Janoš, P.; Ecorchard, P.; Tolasz, J.; Štengl, V.; Beneš, H.; Perchacz, M.; Pop-Georgievski, O. Determination of Amino Groups on Functionalized Graphene Oxide for Polyurethane Nanomaterials: XPS Quantitation vs. Functional Speciation. *RSC Adv.* **2017**, *7* (21), 12464−12473.

(52) Bierbaum, K.; Kinzler, M.; Woell, Ch.; Grunze, M.; Haehner, G.; Heid, S.; Effenberger, F. A Near Edge X-Ray Absorption Fine Structure Spectroscopy and X-Ray Photoelectron Spectroscopy Study of the Film Properties of Self-Assembled Monolayers of Organosilanes on Oxidized Si(100). *Langmuir* **1995**, *11* (2), 512−518.

(53) Zheng, G.; Xiang, Y.; Xu, L.; Luo, H.; Wang, B.; Liu, Y.; Han, X.; Zhao, W.; Chen, S.; Chen, H.; Zhang, Q.; Zhu, T.; Yang, Y. Controlling Surface Oxides in Si/C Nanocomposite Anodes for High-Performance Li-Ion Batteries. *Adv. Energy Mater.* **2018**, *8* (29), 1801718.

(54) Bousiakou, L. G.; Karapetis, S. Determination of Au Film Thiolation and Silane Bonding Onto SiO2 Films Within the Frame of Biosensor Surface Functionalization - an Analysis of Best Practices and Techniques. *Croat. Chem. Acta* **2020**, *93* (1), 1−14.

(55) Zhang, L.; Kuramoto, N.; Kurokawa, A. XPS Analysis of a 28Si-Enriched Sphere for Realization of the Kilogram. *IEEE Trans. Semicond. Manuf.* **2021**, *70*, 1−5.

(56) González-Flores, K. E.; Palacios-Márquez, B.; Álvarez-Quintana, J.; Pérez-García, S. A.; Licea-Jiménez, L.; Horley, P.; Morales-Sánchez, A. Resistive switching control for conductive Si-nanocrystals embedded in Si/SiO₂ multilayers. *Nanotechnology* **2018**, *29* (39), 395203.

(57) Hafeez, H.; Choi, D. K.; Lee, C. M.; Jesuraj, P. J.; Kim, D. H.; Song, A.; Chung, K. B.; Song, M.; Ma, J. F.; Kim, C.-S.; Ryu, S. Y. Replacement of N-Type Layers with a Non-Toxic APTES Interfacial Layer to Improve the Performance of Amorphous Si Thin-Film Solar Cells. *RSC Adv.* **2019**, *9* (13), 7536−7542.

(58) Dietrich, P. M.; Glamsch, S.; Ehlert, C.; Lippitz, A.; Kulak, N.; Unger, W. E. S. Synchrotron-Radiation XPS Analysis of Ultra-Thin

Silane Films: Specifying the Organic Silicon. *Appl. Surf. Sci.* **2016**, *363*, 406−411.

(59) Dang, T. A.; Chau, C. N. Electron Spectroscopy for Chemical Analysis of Cool White Phosphors Coated with SiO2 Thin Film. *J. Electrochem. Soc.* **1996**, *143* (1), 302−305.

(60) Sun, Y.; Yanagisawa, M.; Kunimoto, M.; Nakamura, M.; Homma, T. Estimated Phase Transition and Melting Temperature of APTES Self-Assembled Monolayer Using Surface-Enhanced Anti-Stokes and Stokes Raman Scattering. *Appl. Surf. Sci.* **2016**, *363*, 572−577.

(61) Granneman, E. H. A. Thin Films in the Integrated Circuit Industry: Requirements and Deposition Methods. *Thin Solid Films* **1993**, *228* (1−2), 1−11.

(62) Beena Unni, A.; Winkler, R.; Duarte, D. M.; Chat, K.; Adrjanowicz, K. Influence of Surface Roughness on the Dynamics and Crystallization of Vapor-Deposited Thin Films. *J. Phys. Chem. B* **2022**, *126* (40), 8072−8079.

(63) Zhu, M.; Lerum, M. Z.; Chen, W. How To Prepare Reproducible, Homogeneous, and Hydrolytically Stable Aminosilane-Derived Layers on Silica. *Langmuir* **2012**, *28* (1), 416−423.

(64) Bulou, S.; Lecoq, E.; Loyer, F.; Frache, G.; Fouquet, T.; Gueye, M.; Belmonte, T.; Choquet, P. Study of a Pulsed Post-discharge Plasma Deposition Process of APTES: Synthesis of Highly Organic Pp-APTES Thin Films with NH $_2$ Functionalized Polysilsesquioxane Evidences. *Plasma Process. Polym.* **2019**, *16* (4), 1800177.

(65) Soethoudt, J.; Tomczak, Y.; Meynaerts, B.; Chan, B. T.; Delabie, A. Insight into Selective Surface Reactions of Dimethylami-no-Trimethylsilane for Area-Selective Deposition of Metal, Nitride, and Oxide. *J. Phys. Chem. C* **2020**, *124* (13), 7163−7173.

(66) Soethoudt, J.; Crahaij, S.; Conard, T.; Delabie, A. Impact of SiO2 Surface Composition on Trimethylsilane Passivation for Area-Selective Deposition. *J. Mater. Chem. C* **2019**, *7* (38), 11911−11918.

(67) Zyulkov, I.; Madhiwala, V.; Voronina, E.; Snelgrove, M.; Bogan, J.; O'Connor, R.; De Gendt, S.; Armini, S. Area-Selective ALD of Ru on Nanometer-Scale Cu Lines through Dimerization of Amino-Functionalized Alkoxy Silane Passivation Films. *ACS Appl. Mater. Interfaces* **2020**, *12* (4), 4678−4688.

(68) Dufil, Y.; Gadenne, V.; Carrière, P.; Nunzi, J.-M.; Patrone, L. Growth and Organization of (3-Trimethoxysilylpropyl) Diethylenetri-amine within Reactive Amino-Terminated Self-Assembled Monolayer on Silica. *Appl. Surf. Sci.* **2020**, *508*, 145210.

(69) Vega, A.; Thissen, P.; Chabal, Y. J. Environment-Controlled Tethering by Aggregation and Growth of Phosphonic Acid Monolayers on Silicon Oxide. *Langmuir* **2012**, *28* (21), 8046−8051.

(70) Hotchkiss, P. J.; Jones, S. C.; Paniagua, S. A.; Sharma, A.; Kippelen, B.; Armstrong, N. R.; Marder, S. R. The Modification of Indium Tin Oxide with Phosphonic Acids: Mechanism of Binding, Tuning of Surface Properties, and Potential for Use in Organic Electronic Applications. *Acc. Chem. Res.* **2012**, *45* (3), 337−346.

(71) Cooper, E.; Leggett, G. J. Influence of Tail-Group Hydrogen Bonding on the Stabilities of Self-Assembled Monolayers of Alkylthiols on Gold. *Langmuir* **1999**, *15* (4), 1024−1032.

(72) Liu, H.; Xu, C.-Y.; Du, Y.; Ma, F.-X.; Li, Y.; Yu, J.; Zhen, L. Ultrathin Co9S8 Nanosheets Vertically Aligned on N,S/RGO for Low Voltage Electrolytic Water in Alkaline Media. *Sci. Rep.* **2019**, *9* (1), 1951.

(73) Denayer, J.; Delhalle, J.; Mekhalif, Z. Comparative Study of Copper Surface Treatment with Self-Assembled Monolayers of Aliphatic Thiol, Dithiol and Dithiocarboxylic Acid. *J. Electroanal. Chem.* **2009**, *637* (1−2), 43−49.

(74) Laiho, T.; Leiro, J. A.; Heinonen, M. H.; Mattila, S. S.; Lukkari, J. Photoelectron Spectroscopy Study of Irradiation Damage and Metal-Sulfur Bonds of Thiol on Silver and Copper Surfaces. *J. Electron Spectrosc. Relat. Phenom.* **2005**, *142* (2), 105−112.

(75) Li, Y.; Kong, M.; Hu, J.; Zhou, J. Carbon-Microcuboid-Supported Phosphorus-Coordinated Single Atomic Copper with Ultrahigh Content and Its Abnormal Modification to Na Storage Behaviors. *Adv. Energy Mater.* **2020**, *10* (19), 2000400.